Impact of Variability, Uncertainty and Frequency Regulation on Power System Frequency Distribution

Francesca Madia Mele[1], Álvaro Ortega[1], Rafael Zárate-Miñano[2], Federico Milano[1*]
[1]School of Electrical and Electronic Engineering, University College Dublin, Dublin, Ireland
[2]Dept. of Electrical Engineering, University of Castilla - La Mancha, Almadén, Spain
*Corresponding author: federico.milano@ucd.ie

***Abstract*—This work originates from the observation of the frequency distribution of the Irish system as obtained from a Frequency Disturbance Recorder lent to the last author by the University of Tennessee. The probability density function of such a distribution appears to be bimodal. The paper first investigates how stochastic sources, in particular, load and wind power estimation errors, impact on the distribution of the frequency of a high-voltage transmission system. Then, possible routes to obtain a bimodal distribution of the frequency are explored and the most likely cause that leads to the observed behaviour of the Irish system is identified. Finally, the paper presents a comparison of different frequency regulation strategies and their impact on the distribution of the frequency. A sensitivity analysis of wind speed and load parameters is presented and discussed based on the IEEE-14 bus system.**

I. Introduction

A. Motivation

The stochastic behaviour of the power generation of wind power plants, along with the variability and uncertainty of demand, have an impact on the dynamic behaviour of the power system, affecting both frequency and voltage stability. For this reason, in recent years, there has been a growing interest in understanding the impact of such randomness into the system. Within this framework, a Frequency Disturbance Recorder (FDR) has been lent to the last author from the Power system Group led by Prof. Yilu Liu, University of Tennessee, Knoxville [1]. The FDR is a FNET/GridEye device, developed at Virginia Tech, that measures the frequency, phase angle, and voltage of the power signal found at ordinary electrical outlets. The main goal of the FNET project is to register and analyze frequency variations following large disturbances [2], [3]. In this paper, we follow a different approach. We have stored the measurements of the FDR, which has a sampling rate of 0.1 s and an accuracy of 0.0001 Hz, during a large period, i.e., one year at the time of writing this paper. The goal is to analyze the statistical properties of a large time series with high resolution.

Figure 1 shows the probability density of the frequency during a sample week. The frequency distribution is bimodal and not, as expected, normal. The interested reader can find more details on the behaviour of the frequency distribution in the Irish system in [4]. The normal distribution is actually the common assumption for the design of system controllers and statistical analysis. Based on this unexpected observation, this paper is aimed to investigate the causes that lead to such a bimodal distribution. Moreover, the paper also discusses the effect of non-conventional frequency controllers that can mitigate the bimodal distribution of the frequency and recover the usual normal one.

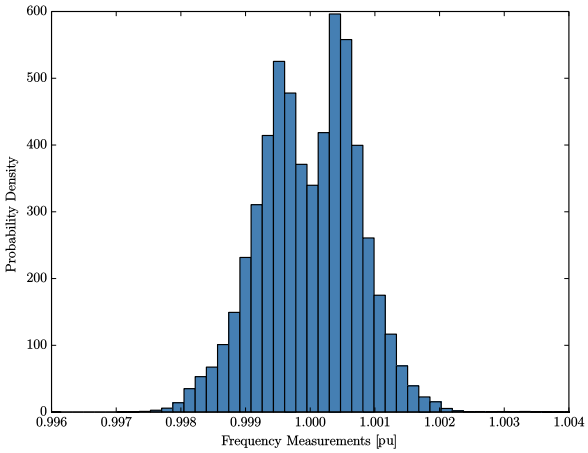

Figure 1: Probability density of the frequency of the Irish system measured with the FDR from the 11th to the 17th of August 2014.

B. Background and Literature Review

The increasing penetration of variable non-synchronous wind generation in power systems creates new challenges for the operation and control of the network, such as maintaining system frequency within acceptable values, while coping with fluctuations in demand and generation sides [5]. In several systems, like for example in the US, it has also been observed a reduction of the primary frequency regulation, thus leading to a poorer dynamic response of the system to power mismatches due to the variability and uncertainty of the load and non-dispatchable generation [6], [7]. It is also well-known that, as the penetration of distributed energy resources in power systems increases, their potential to provide ancillary services becomes more and more significant but, at the same time, new challenges related to frequency regulation of the grid arise [8].

In this paper, we are interested in defining the causes of the bimodal distribution of the frequency shown in Fig. 1. With this aim, it is required to have a proper model of the system, not only in terms of dynamic machine models and controllers,

but also in terms of the stochastic perturbations that affect the system itself. In particular, we are interested in modelling the impact of the power mismatches caused by the variability and/or uncertainty of the load demand, on one hand, and the wind power generation on the other hand. These are the two main sources of randomness considered in this paper as these are the ones that can be found in the Irish system.

We thus need reasonable models of stochastic processes to simulate power estimation errors. In [9], an innovative method based on Stochastic Differential Equations (SDEs) to model power systems affected by stochastic perturbations is proposed, whereas [10] uses SDEs to model the variability in wind power generation. With respect to load, its dynamic behaviour can be described, with a good level of approximation, by an Ornstein-Uhlenbeck process [11].

In the second part of this paper, we analyze the effect of non-conventional frequency regulation strategies on the distribution of the frequency. Such regulations are based on frequency controllers proposed and discussed in [12]–[14]. These are coupled to the following devices: (i) variable-speed wind power plants; (ii) thermostatically controlled loads; and (iii) energy storage devices. We also consider the effect of the secondary frequency control, although such a control is currently not included in the Irish system.

C. Contributions

The main contributions of the paper are as follows.

- Identify, through a comprehensive sensitivity analysis and time domain simulation based on SDEs, the causes that lead to the bimodal distribution of the frequency shown in Fig. 1.
- Compare the impact on the frequency distribution of different frequency regulation strategies.

D. Paper Organization

The paper is organized as follows. Section II presents the theoretical background of the SDEs that are proposed to model load and wind power estimation errors and that are used in the case study. Section III outlines the non-conventional frequency controllers. Section IV duly discusses the case study based on the IEEE 14-bus system. Finally, Section V draws relevant conclusions and suggests applications of the findings of the paper and future work directions.

II. Modelling of Load and Wind Power Estimation Errors

For the purpose of introducing the discussion of the case study included in Section IV, this section presents the proposed models of the estimation errors of load demand and wind speed. We consider two kinds of errors, as follows:

- Uncorrelated errors. These are modelled using SDEs whose diffusion terms are uncorrelated. This model allows capturing stochastic fluctuations in terms of both variability (fluctuations around an average estimated value) and uncertainty (deviations from the average estimated value).
- Correlated errors. These models capture systematic estimation errors in the forecast and are thus only related to uncertainty. We assume that these errors are common to the whole system and are characterized by a periodic behavior. Such a periodicity does not model a specific phenomenon, but rather simulates the main harmonic of correlated estimation errors.

A. Modelling of Uncorrelated Errors

In this paper, stochastic perturbations, i.e., wind speed and load demand estimation errors, are modelled through an Ornstein-Uhlenbeck Process (OUP), also known as *mean-reverting* process [15]. The OUP has already been used in the literature to formulate a stochastic model of the power system loads [9], [11]. The main feature of the OUP that makes it interesting in this context is its property to keep the standard deviation bounded. This appears as a sensible feature in several physical processes, where the variability and/or uncertainty does not increase with time.

The OUP is modelled in this paper as a SDE, as follows:

$$\dot{\eta}(t) = \alpha(\mu - \eta(t)) + b\xi \tag{1}$$

where $\eta(t)$ is the stochastic variable whose time evolution is driven by the *drift* term $\alpha(\mu - \eta(t))$ and the *diffusion* term, b, of the SDE; α is the mean reversion speed that dictates how quickly the $\eta(t)$ tends to the given mean value μ. Finally, ξ is the white noise, formally defined as the time derivative of the Wiener process.

The use of continuous SDEs appears as a natural choice as the standard power system model for transient angle and voltage stability analyses is based on Differential Algebraic Equations (DAEs) which can be assumed continuous except for a reduced set of discrete events [16]. The interested reader can find further discussion on the modelling of power systems as a set of stochastic DAEs (SDAEs) in [9].

We assume that the wind speed estimated error and the load forecast error can be modelled as a normal distribution [17]. With this aim, model (1) is adequate to describe the estimation errors due to the mismatch between the *forecast* and the *actual* values of both demands and wind power generations. These errors lead to a power mismatch that has to be compensated by the primary frequency regulation of synchronous machines and of other devices, if available. Note that these estimation errors do not depend on the particular characterizations of the wind distribution nor to the nature of the load profile. For example, the wind speed is known not to follow a normal distribution, but rather a Weibull or other asymmetrical distributions (e.g., see [18] and [19]).

Based on the above, the proposed model of fully uncorrelated estimation errors of load demand is a set of SDAEs based on the OUP, as follows:

$$\begin{aligned} p_L(t) &= (p_{L0} + \eta_p(t))(v(t)/v_0)^\gamma \\ \dot{\eta}_p(t) &= \alpha_p(\mu_p - \eta_p(t)) + b_p\xi_p \end{aligned} \tag{2}$$

where p_L and p_{L0} are the active power of the loads and their initial active load power, respectively; v and v_0 are the voltage

magnitude at the bus where the load is connected and its initial value, respectively; and γ is a parameter that defines the dependence of the load on the voltage. Finally, η_p, α_p, μ_p, b_p and ξ_p have same meaning as in (1). A similar model is assumed for the estimation error of load reactive powers (characterized by variables q_L, η_q and ξ_q and parameters q_{L0}, α_q, μ_q and b_q). Similarly, the wind speed $w_s(t)$ that feeds the wind turbine models is modelled as:

$$w_s(t) = w_{s0} + \eta_w(t) \tag{3}$$
$$\dot{\eta}_w(t) = \alpha_w(\mu_w - \eta_w(t)) + b_w\xi_w$$

where variables and parameters have analogous meanings as in (2).

B. Modelling of Correlated Errors

For the sake of the sensitivity analysis carried out in the case study, fully correlated estimation errors related to the load demand are modelled as in (2), where μ_p is a time-varying mean value according to:

$$\mu_p(t) = \mu_{pc} sin(\omega_c t + \phi_c) \tag{4}$$

where μ_{pc} is the amplitude of a given oscillation with frequency ω_c and phase ϕ_c. The correlated estimation errors related to reactive powers and wind speed can be modelled using similar expressions as (4) with amplitude μ_{qc} and μ_{wc}, respectively.

The assumption is that the phase ϕ_c is the same for all load power demands and/or wind speeds, thus leading to a fully correlated "oscillation" of the estimation error of the load demand. We assume that such oscillation is an harmonic content of the overall estimation error, due for example, to some systematic error of the forecast or measurement system. Hence, in the case study, (4) is coupled with the stochastic model provided by (2).

III. Primary, Secondary and Non-conventional Frequency Controllers

This section outlines the primary frequency controller of conventional power plants based on synchronous machines as well as a variety of frequency controllers that are considered in the case study below. The considered devices and controllers are:

- Synchronous machine Turbine Governor (TG)
- Automatic Generation Control (AGC)
- Wind Energy Conversion System (WECS)
- Thermostatically Controlled Load (TCL)
- Energy Storage System (ESS).

A. Synchronous machine Turbine Governor

A typical primary frequency control scheme of a conventional power plant is shown in the upper scheme of Fig. 2 [20]. It includes a governor, a servo and a reheat block. The lower scheme depicted in Fig. 2 shows the same controller with inclusion of a deadband on the frequency error signal. As stated in [21]: *The general industry mindset for governor deadbands is to minimize generator movement due to frequency regulation. This may work for an interconnection where generators have various deadband settings. But when a majority of the generators set the deadband exactly the same and with a step function, the benefit completely disappears because frequency will move to the deadband frequently.* The concept above is further discussed and illustrated through the simulations provided in the case study.

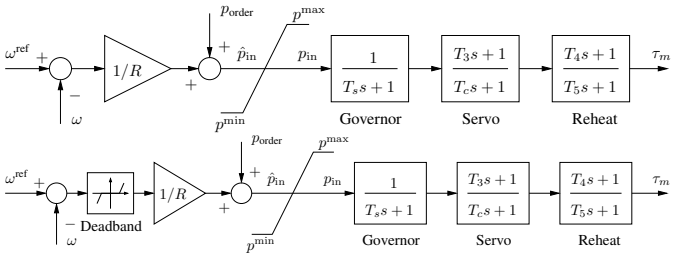

Figure 2: Turbine governor. Upper scheme: conventional scheme without deadband. Lower scheme: scheme with inclusion of a deadband on the frequency error signal.

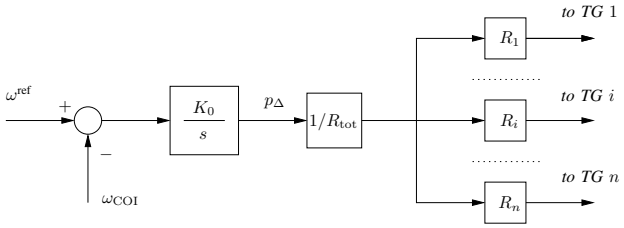

Figure 3: Simple automatic generation control scheme.

B. Automatic Generation Control

A simple AGC scheme, which is the one used for the case study of this paper, is depicted in Fig. 3 [22]. From the control viewpoint, the main purpose of the AGC is to provide a perfect tracking of the reference frequency. However, to maintain the stability of the primary frequency regulation, the AGC has to be an order of magnitude slower than the primary frequency control provided by the turbine governor. The AGC includes an integral controller to take the frequency error to zero in steady-state. The measured speed is that of the centre of inertia (ω_{COI}) or of a pilot bus of the system. In Fig. 3, K_0 is the integral gain and ω^{ref} is the reference frequency, which typically coincides with the nominal synchronous speed of the system. In the scheme of Fig. 3, the AGC coordinates n turbine governors. Then, $R_{\text{tot}} = \sum_{i=1}^{n} R_i$, where R_i is the droop of turbine governor i.

C. Frequency Regulation of Wind Turbines

The possibility and need that WECSs provide primary frequency regulation support has been widely discussed in recent years [8]. This would allow reducing the impact of intermittent energy resources as well as compensate the loss of primary frequency regulation of the conventional synchronous machines whose place is taken by such non-dispatchable sources. While in real-world systems (e.g., the Irish one), wind power plants do not actually participate to the primary

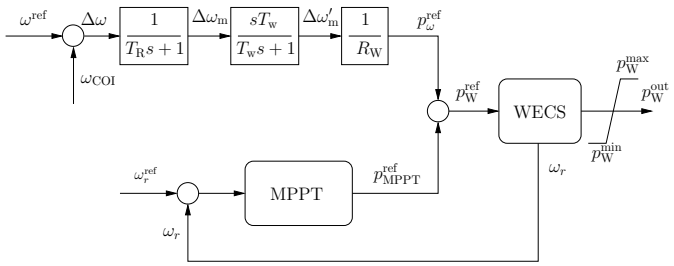

Figure 4: Primary frequency controller for a variable-speed wind turbine.

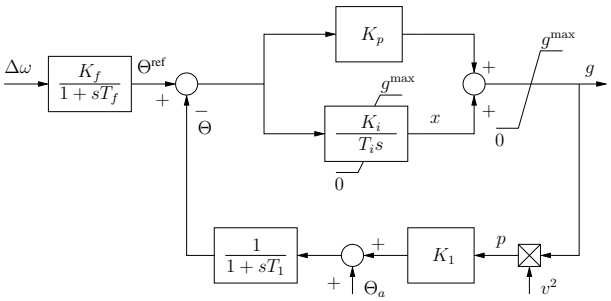

Figure 5: Thermostatically controlled load with frequency control.

frequency regulation, this situation is anticipated to change in the near future.

In the case study, we consider a transient primary frequency control of wind power plants similar to that proposed in [23]. Such a control is shown in Fig. 4. It takes and filters a measure of the system frequency deviation $\Delta\omega$ at the point of connection of the WECS and then modifies the set point of the maximum power point tracking (MPPT) controller. Clearly, only variable speed wind turbines, such as doubly-fed induction generators or direct-drive synchronous machines can provide primary frequency regulation. Several other control schemes have been proposed, mostly based on the somewhat misleading concept of *emulated inertia* [24]. A discussion on the advantages and drawbacks of different control strategies of wind power plants is, however, beyond the scope of this paper.

D. Thermostatically Controlled Loads

TCLs are dynamic loads with temperature control [25]. These can be air conditioning systems, industrial refrigerators or heating systems. In most cases, the reference temperature is fixed to an assigned value. There are, however, experimental prototypes of thermostatically controlled loads that include a measure of the system frequency and that vary the reference temperature in order to reduce frequency deviations [26], [27].

The control scheme of the TCL is depicted in Fig. 5. The meaning of the variables are the following: Θ is the load temperature (lumped model); Θ_a is the ambient temperature; g is the equivalent load conductance, v is the load terminal voltage; and p the consumed active power. The frequency deviation $\Delta\omega$ is measured at the connection bus through a washout filter [28].

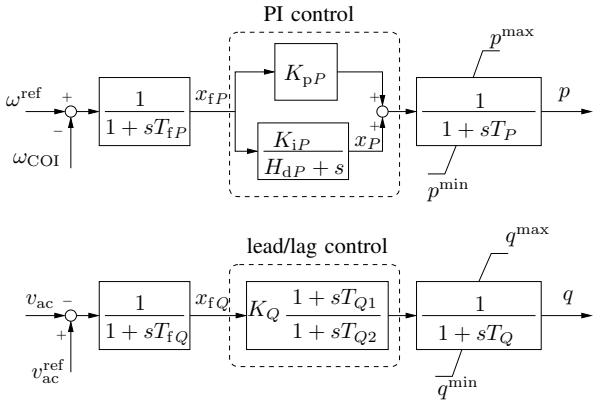

Figure 6: Control scheme of a converter-based energy storage system with frequency and voltage control.

E. Model of the Energy Storage System

In recent years, several energy storage technologies have been investigated. These include the Superconducting Magnetic Energy Storage (SMES), the Compressed Air Energy Storage (CAES) and the Battery Energy Storage (BES) [29]. All systems above are coupled to the ac grid through VSC devices. The idea that energy storage devices could be used for frequency regulation in power systems is supported in the literature, e.g., [14] and [30].

A commonly-used model of ESSs is presented in Fig. 6 [28], [31]. The purpose of this device is to regulate the frequency of the system, ω_{COI}, through the active power provided/consumed by the ESS, p, as well as the ac voltage at the point of connection of the storage device with the rest of the system, v_{ac}, by means of the reactive power, q. The deviations of both ω_{COI} and v_{ac} with respect to their reference values, ω^{ref} and $v_{\mathrm{ac}}^{\mathrm{ref}}$, are passed through low pass filters and regulated by means of a PI and a lead/lag controllers, respectively. Finally, the physical behavior of the ESS is represented by the time constants T_P and T_Q.

IV. Case Study

The objective of this section is twofold. Subsection IV-B investigates how it is possible to obtain a bimodal distribution of the frequency of the system. Subsection IV-C presents a comprehensive analysis of the effect of different frequency regulation strategies on the frequency distribution.

The well-known IEEE 14-bus system is used for all simulations of this section. Such a benchmark includes 2 synchronous machines, 3 synchronous compensators, 2 two-winding and 1 three-winding transformers, 15 transmission lines, 11 static loads totaling 259 MW and 81.3 MVAr as well as standard primary frequency and voltage regulators. All dynamic data of the IEEE 14-bus system as well as a detailed discussion on its stability can be found in [32].

We use the IEEE 14-bus system to emulate on a small scale the behaviour of the Irish system and, hence, qualitatively reproduce the empirical frequency distribution shown in Fig. 1. With this aim, some modifications are made to the original setup of the IEEE 14-bus system, as follows:

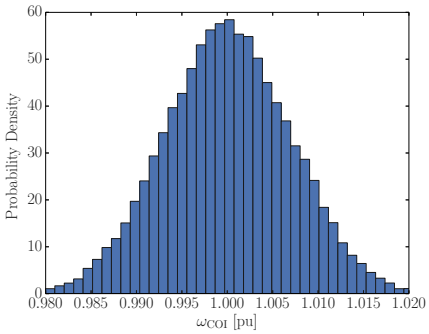

Figure 7: IEEE-14 bus system – Distribution of the frequency of the COI considering primary frequency regulation and uncorrelated stochastic variations of the load.

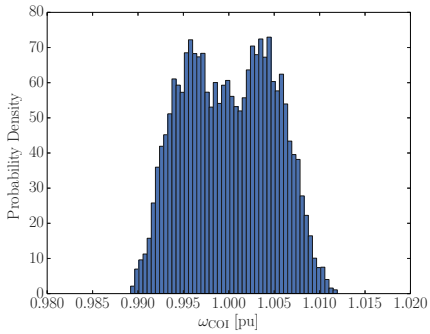

Figure 8: IEEE 14-bus system – Distribution of the frequency of the COI considering primary frequency regulation ($R = 0.05$) and correlated estimation errors of load power consumption ($\mu_{pc} = \mu_{qc} = 5\%$).

- The synchronous machine on bus 2 is replaced with a wind power plant represented by an aggregated model with a nominal capacity of 40 MW. The aggregated model implements a 10-th order Doubly-Fed Induction Generator (DFIG) with voltage, pitch angle and MPPT controllers.
- The inertia of the machine on bus 1 is reduced by 6 times.

The analysis is based on time domain simulations and all simulations are 24-hour long with a time step of 0.1 s.

All simulations are obtained using Dome, a Python and C-based software tool that allows simulating large power systems modelled as a set of SDAEs [33]. The Dome version used for this case study is based on Python 3.4.1; ATLAS 3.10.1 for dense vector and matrix operations; CVXOPT 1.1.7 for sparse matrix operations; and KLU 1.3.2 for sparse matrix factorization. All simulations were executed on a 64-bit Linux Fedora 21 operating system running on two Intel Xeon 10 Core 2.2 GHz CPUs and 64 GB of RAM.

A. Base case

Figure 7 shows the distribution of the frequency of the IEEE 14-bus system assuming a set of stochastic disturbances modelled as in (2) and (3) and applied to both wind speed ($b_w = 1\%$, $\alpha_w = 0.003$ pu/s) and load active and reactive powers ($b_p = b_q = 1\%$ and $\alpha_p = \alpha_q = 0.02$ pu/s). As expected, the probability density of the frequency of the COI resembles a normal distribution. This is also the common understanding of the behaviour of the frequency but, clearly, it does not match the distribution of the experimental measurements of Fig. 1. The cause that leads to the bimodal distribution has thus to be further investigated.

B. Bimodal distribution of the frequency of the network

We have found, empirically, two possible routes to obtain a bimodal distribution of the frequency, as follows:

- A periodic oscillation of the estimation error of the wind speed and/or the load power consumption;
- A deadband included into the primary frequency regulation of synchronous machines.

To prove the statements above, we proceed using a parametric analysis based on the primary frequency control of the conventional power plant of the IEEE 14-bus system.

1) Periodic oscillation of the estimation error of load demand: In this scenario, all load active and reactive powers are assumed to vary coherently according to (4) with $\omega_c = 0.0033$ Hz and $\mu_{pc} = \mu_{qc} = 5\%$. For simplicity, but without lack of generality, the estimation error of the wind speed is assumed to be an uncorrelated OUP with same parameters as in the base case. The resulting probability density of the frequency of the COI is shown in Fig. 8. The two peaks of the distribution denote a fluctuation of the frequency within a range following the oscillation of the load estimated error.

Varying the parameters of the system, such as the droop of the turbine governor or the amplitude of the estimated error of the load, the distance between the two peaks changes significantly, while the bimodal shape is preserved. For example, Fig. 9 shows the distribution of the frequency of the COI for a primary frequency control with a droop 5 times smaller than the base case one, i.e., $R = 0.01$. Note that the frequency tends to concentrate around the nominal frequency, and hence, the standard deviation decreases. The smaller the droop the closer to a normal distribution is the probability density of the system frequency. Figure 10 shows the effect of varying the amplitude of the estimation error of the load power consumption ($\mu_{pc} = \mu_{qc} = 8\%$) on the distribution of the frequency. As expected, the bigger the amplitude of the estimation error, the higher is the standard deviation of the frequency.

2) Primary frequency regulation with deadband: As mentioned above, the bimodal shape of the frequency distribution can be a result of the inclusion of a deadband into the primary frequency regulators of synchronous machines. Note, however, that the bimodal distribution appears only if all primary regulators use exactly the same value of the deadband [21]. Figure 11 shows the distribution of the frequency for a typical deadband value, i.e., $db = 0.0006$ pu (Hz), and $R = 0.05$ for the primary frequency regulator of the machine connected to bus 1, while Fig. 12 shows the COI frequency distribution with same deadband and droop $R = 0.01$. The parameters of

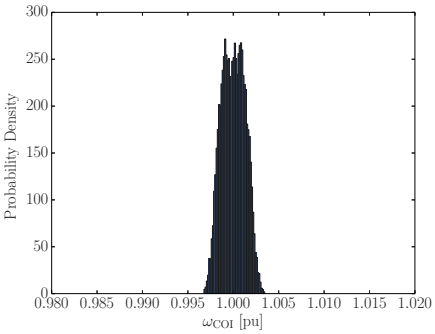

Figure 9: IEEE 14-bus system – Distribution of the frequency of the COI considering primary frequency regulation ($R = 0.01$) and correlated estimation errors of load power consumption ($\mu_{pc} = \mu_{qc} = 5\%$).

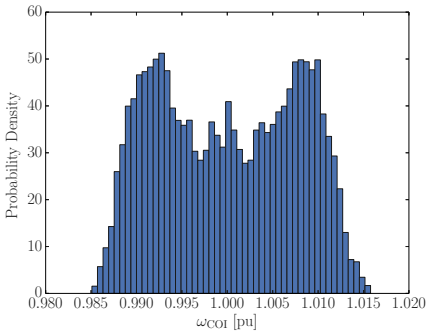

Figure 10: IEEE 14-bus system – Distribution of the frequency of the COI considering primary frequency regulation ($R = 0.05$) and correlated estimation errors of load power consumption ($\mu_{pc} = \mu_{qc} = 8\%$).

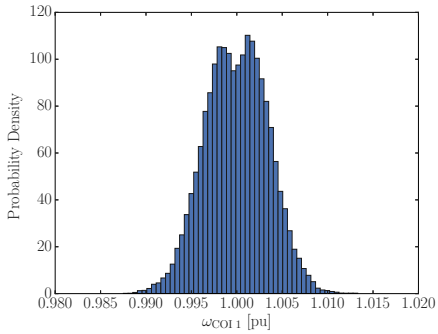

Figure 11: IEEE 14-bus system – Distribution of the frequency of the COI considering primary frequency regulation with with $R = 0.05$ and $db = 0.0006$ pu, and uncorrelated stochastic load variations.

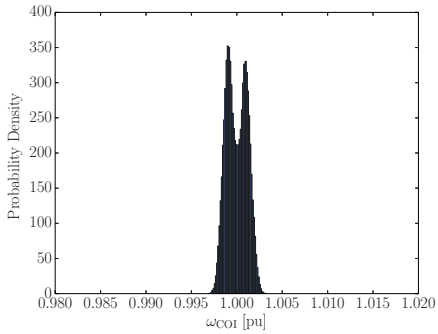

Figure 12: IEEE 14-bus system – Distribution of the frequency of the COI considering primary frequency regulation with $R = 0.01$ and $db = 0.0006$ pu, and uncorrelated stochastic load variations.

stochastic perturbations are the same as in the base case, except for the mean-reversion speed of load estimation errors, which in this case are set as $\alpha_p = \alpha_q = 2$ pu/s. Note that the bimodal distribution disappears for smaller values of the deadband [21] as well as for smaller values of the mean-reversion speeds.

C. Comparison of frequency controllers

In this Section a comparison of the impact of the frequency controllers described in Section III is performed. Two scenarios are taken into account: the Base Case depicted in Section IV-A, and the inclusion of a deadband into the primary frequency regulators of synchronous machines. For space limitations, we focus only on the latter, because it is very likely that this causes the bimodal we observe in the behaviour of the Irish system. Results related to the cyclic variation of the loads lead to similar conclusions.

All simulations are carried out considering a turbine governor with $R = 0.05$. For the simulations including the deadband, a typical deadband value is chosen, i.e., $db = 0.0006$ pu (Hz). Stochastic processes of the estimation errors of both loads and wind speed are modelled using same parameters as for the base case.

Relevant parameters of the considered frequency controllers are as follows.

- The gain of the AGC is $K_0 = 10$.
- The time constants of the frequency washout filter of the WECS is $T_w = 10.0$ s.
- 20% of the loads are assumed to include a TCL with frequency control. The proportional and integral gains of the TCL are $K_p = 100$ and $K_i = 25$; and the thermal load time constant is $T_1 = 1200$ s.
- Two ESSs are considered: (i) a BES that simulates a "slow" control ($T_P = 8$ s); and (ii) a SMES that simulates a "fast" control ($T_P = 0.8$ s). No saturation of ESS devices is considered.

Figures 13 to 15 show the effect of each frequency controller normalized with respect to the base case scenario. As expected, the faster the control, the narrower is the range within which the frequency fluctuates (see also Table I and Table II).

If a deadband in the primary frequency regulation is considered, the frequency can be described by a bimodal distribution. Assuming both unimodal distributions to be normal, the resulting bimodal is:

$$p(x) = \omega N_1(\mu_1, \sigma_1) + (1 - \omega) N_2(\mu_2, \sigma_2) \tag{5}$$

where ω is the mixing parameter, μ_1 and μ_2, σ_1 and σ_2 are the mean value and the standard deviation of each unimodal, respectively. Note that, the slower the control, the deeper the valley between the two peaks.

In Fig. 13, the base case is compared with the scenarios with AGC, WECS and TCL devices. The latter two do not

Scenario	σ [10^{-3} pu]	Scenario	σ [10^{-3} pu]
Base Case	6.67	BES	3.56
AGC	3.37	SMES	2.99
WECS	6.01	All-BES	1.59
TCL	5.15	All-SMES	1.52

TABLE I: IEEE 14-bus system – Standard deviations of the frequency distributions for different frequency controllers with no deadband.

Scenario	μ_1	σ_1 [10^{-3} pu]	μ_2	σ_2 [10^{-3} pu]
Base Case	0.997181	2.015	1.002770	1.966
AGC	1	1.751		
WECS	0.997449	1.845	1.002510	1.799
TCL	0.997770	1.639	1.002180	1.560
BES	0.999000	1.040	1.001500	1.016
SMES	0.999000	0.888	1.001000	0.855
All-BES	1	0.822		
All-SMES	1	0.780		

TABLE II: IEEE 14-bus system – Standard deviations of the frequency distributions for different frequency controllers. Synchronous machine primary frequency regulation includes a deadband ($db = 0.0006$ pu).

lead to substantial changes with respect to the base case. The TCL, in fact, is too slow, whereas the WECS has too limited regulating capacity. On the other hand, the AGC consistently reduces the fluctuations of the frequency of the COI – the standard deviation of the frequency is 4 times smaller than that of the base case (see Table I). Similar remarks can be drawn if a deadband is included in the primary frequency regulators of the synchronous machines. The bimodal distribution is preserved for all frequency controller, except for the AGC. The integral control of the AGC, in fact, perfectly tracks the reference synchronous speed and leads to a normal distribution of the system frequency.

Figure 14 shows the comparison of the base case with the ESS devices. Both devices are faster than the primary frequency regulation of the synchronous machines and, thus, reduce the fluctuations of the frequency with respect to the base case. Note, however, that this is an ideal scenario as the ESSs are assumed to have unlimited storage capacity.

The combined effect of all frequency controllers is shown in Fig. 15. As expected, the frequency fluctuates in a very small range, whether the deadband is taken into account or not. Despite the relatively different time responses, the performances of the ESSs when combined with other frequency controllers are almost identical. In fact, even in case a deadband is included, ESS control is so fast that the valley between the two peaks disappears, and the bimodal distribution turns into a normal.

V. Conclusions

This paper presents a sensitivity analysis of the parameters that impact on the distribution of the frequency of a high-voltage transmission system. As expected, the variability and uncertainty, modelled as mean-reverting processes, of load and wind leads to a normal distribution. Then, possible routes that lead to obtain a bimodal distribution appear to be a periodic oscillation, which models forecast uncertainty, of load powers and/or wind speed estimation errors and a deadband in the

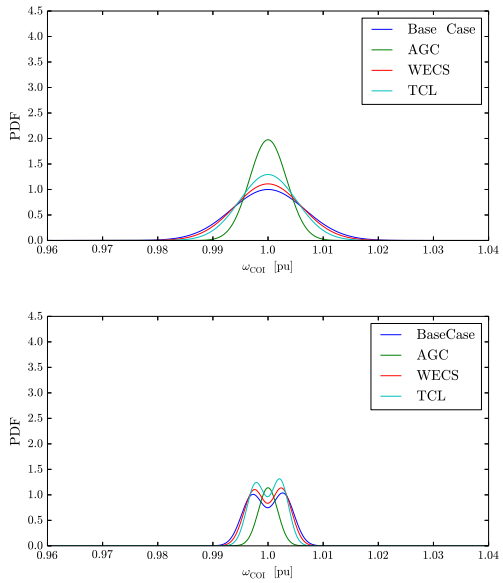

Figure 13: PDFs of frequency of the COI for the IEEE 14-bus system. Comparison of the following frequency control strategies with the base case: AGC, WECS, TCL. Upper panel: base case scenario with no deadband; lower panel: primary frequency regulation with $db = 0.0006$ pu

.

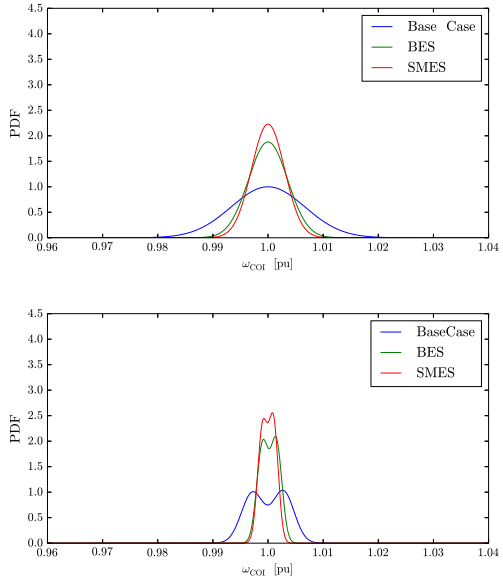

Figure 14: PDF of frequency of the COI for the IEEE 14-bus system. Comparison of the following frequency control strategies with the base case: ESS devices (BES and SMES considered separately). Upper panel: base case scenario with no deadband; lower panel: primary frequency regulation with $db = 0.0006$ pu.

frequency regulation. The latter is often implemented in real-world systems and appears to be *robust* as it is weakly affected by system parameter variations.

The impact of different control strategies is also explored in the paper. As expected, the faster the frequency control and the more the frequency regulators included in the system,

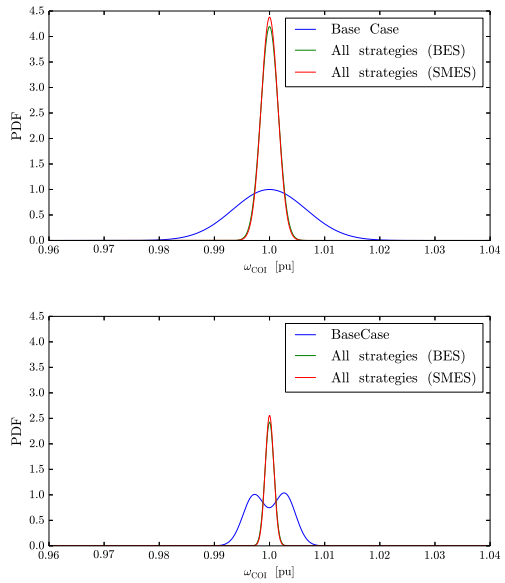

Figure 15: PDF of frequency of the COI for the IEEE 14-bus system. Comparison of the following frequency control strategies with the base case: All strategies implemented (BES and SMES considered separately). Upper panel: base Case scenario with no deadband; lower panel: primary frequency regulation with $db = 0.0006$ pu.

the lower the standard deviation of the frequency distribution, which, in turn, implies a higher power quality of the system.

We see at least two relevant applications of the results obtained in this paper. On one hand, if the frequency controllers implemented in the system are known with accuracy, the analysis of the statistical properties of the frequency distribution can be used for defining the errors of estimation of load demand and/or wind power generation. On the other hand, if the estimation errors are known, the shape of the frequency distribution can reveal the quality and quantity of primary and secondary frequency controls applied to a power system. Future work will focus on the latter application.

REFERENCES

[1] L. Wang and et al., "Frequency Disturbance Recorder Design and Developments," *IEEE PES General Meeting*, pp. 1–7, 2007.

[2] Y. Lei and Y. Liu, "The Impact of Synchronized Human Activities on Power System Frequency," in *IEEE PES General Meeting*, National Harbor, MD, Jul. 2014.

[3] L. Zhan and et al., "Improvement of Timing Reliability and Data Transfer Security of Synchrophasor Measurements," *IEEE PES T&D Conference and Exposition*, pp. 1–5, 2014.

[4] F. Milano, R. Zárate-Miñano, and F. M. Mele, "Characterization of Wind Power Fluctuations from Frequency Measurement Data," in *13th Wind Integration Workshop*, 2014.

[5] EirGrid and SONI, *DS3: Frequency Control Workstream*, 2011.

[6] S. Virmani, "Security Impacts of Changes in Governor Response," in *IEEE PES Winter Meeting*, vol. 1, 1999, pp. 597–599 vol.1.

[7] R. P. Schulz, "Modeling of Governing Response in The Eastern Interconnection," in *IEEE PES Winter Meeting*, vol. 1, 1999, pp. 561–566 vol.1.

[8] G. Lalor, A. Mullane, and M. O'Malley, "Frequency Control and Wind Turbine Technologies," *IEEE Trans. on Power Systems*, vol. 20, no. 4, pp. 1905–1913, 2005.

[9] F. Milano and R. Zárate-Miñano, "A Systematic Method to Model Power Systems as Stochastic Differential Algebraic Equations," *IEEE Trans. on Power Systems*, vol. 28, no. 4, pp. 4537–4544, 2013.

[10] R. Zárate-Miñano, M. Anghel, and F. Milano, "Continuous Wind Speed Models Based on Stochastic Differential Equations," *Applied Energy, Elsevier*, vol. 104, pp. 42–49, 2013.

[11] M. Perninge, V. Knazkins, M. Amelin, and L. Söder, "Risk Estimation of Critical Time to Voltage Instability Induced by Saddle-Node Bifurcation," *IEEE Trans. on Power Systems*, vol. 25, no. 3, pp. 1600–1610, 2010.

[12] J. Mauricio, A. Marano, A. Gomez-Esposito, and J. M. Ramos, "Frequency Regulation Contribution Through Variable-Speed Wind Energy Conversion Systems," *IEEE Trans. on Power Systems*, vol. 24, no. 1, pp. 173–180, 2009.

[13] D. Callaway, "Tapping the Energy Storage Potential in Electric Loads to Deliver Load Following and Regulation, with Application to Wind Energy," *Energy Conversion and Management*, vol. 50, no. 5, pp. 1389–1400, 2009.

[14] A. Ortega and F. Milano, "Design of a Control Limiter to Improve the Dynamic Response of Energy Storage Systems," in *IEEE PES General Meeting*, 2015.

[15] D. T. Gillespie, "Exact Numerical Simulation of the Ornstein-Uhlenbeck Process and its Integral," *Physical Review E*, vol. 54, no. 2, pp. 2084–2091, 1996.

[16] I. A. Hiskens, "Power System Modeling for Inverse Problems," *IEEE Trans. on Circuits and Systems - I: Regular Papers*, vol. 51, no. 3, pp. 539–551, Mar. 2004.

[17] K. Methaprayoon, W. Lee, C. Yingvivatanapong, and J. Liao, "An Integration of ANN Wind Power Estimation into UC Considering the Forecasting Uncertainty," in *Industrial and Commercial Power Systems Technical Conference, 2005 IEEE*, 2005, pp. 116–124.

[18] D. Ke, W. Shi, Z. Bie, C. Liu, X. Rong, and W. Sun, "Probability Modeling on Multiple Time Scales of Wind Power Based on Wind Speed Data," in *PowerCon*, 2014, pp. 2590–2595.

[19] H. Louie, "Evaluation of Probabilistic Models of Wind Plant Power Output Characteristics," in *PMAPS*, 2010, pp. 442–447.

[20] F. Milano, *Power System Modelling and Scripting*. Springer, 2010.

[21] I. Abdur-Rahman, S. Niemeyer, and R. Vera, "Frequency Regulation: Is Your Plant Compliant?" *Power Engineering*, 2010, available at www.power-eng.com.

[22] P. Kundur, *Power System Stability and Control*. EPRI Electric Power Research Institute, McGraw Hill, 2006.

[23] J. M. Mauricio, A. Marano, A. Gómez-Expósito, and J. M. Ramos, "Frequency Regulation Contribution Through Variable-Speed Wind Energy Conversion Systems," *IEEE Trans. on Power Systems*, vol. 24, no. 1, pp. 173–180, 2009.

[24] M. Arani and E. El-Saadany, "Implementing Virtual Inertia in DFIG-Based Wind Power Generation," *IEEE Trans. on Power Systems*, vol. 28, no. 2, pp. 1373–1384, 2013.

[25] P. Hirsch, *Extended Transient-Midterm Stability Program (ETMSP), Ver.3.1 User's Manual*, EPRI, 1994.

[26] S. E. Z. Soudjani and A. Abate, "Aggregation of Thermostatically Controlled Loads by Formal Abstractions," in *European Control Conference (ECC)*, 2013, pp. 4232–4237.

[27] J. L. Mathieu, S. Koch, and D. S. Callaway, "State Estimation and Control of Electric Loads to Manage Real-Time Energy Imbalance," *IEEE Trans. on Power Systems*, vol. 28, no. 1, pp. 430–440, 2013.

[28] F. Milano, *Control and Stability of Future Transmission Networks*. John Wiley & Sons, 2015, in "The Handbook of Clean Energy Systems", editor Prof. Jinyue Yan.

[29] H. T. Le, S. Santoso, and T. Q. Nguyen, "Augmenting Wind Power Penetration and Grid Voltage Stability Limits Using ESS: Application, Design, Sizing, and a Case Study," *IEEE Trans. on Power Systems*, vol. 27, no. 1, pp. 161–171, 2010.

[30] L. Liang, J. Zhong, and Z. Jiao, "Frequency Regulation for a Power System with Wind Power and Battery Energy Storage," in *PowerCon*, 2012, pp. 1–6.

[31] B. C. Pal, A. H. Coonick, I. M. Jaimoukha, and H. El-Zobaidi, "A Linear Matrix Inequality Approach to Robust Damping Control Design in Power Systems with Superconducting Magnetic Energy Storage Device," *IEEE Trans. on Power Systems*, vol. 15, no. 1, pp. 356–362, Feb. 2000.

[32] S. K. M. Kodsi and C. A. Cañizares, *Modeling and Simulation of IEEE 14-bus System with FACTS Controllers*, University of Waterloo, Waterloo, Tech. Rep 2003-3, 2003.

[33] F. Milano, "A Python-based Software Tool for Power System Analysis," in *IEEE PES General Meeting*, Vancouver, BC, Jul. 2013.